Agricultural and Forest Meteorology 279 (2019) 107758

Contents lists available at ScienceDirect

Agricultural and Forest Meteorology

journal homepage: www.elsevier.com/locate/agrformet

Autumn phenology of a temperate deciduous forest: Validation of remote sensing approach with decadal leaf-litterfall measurements

Fan Liu[a,b], Xingchang Wang[a,b,*], Chuankuan Wang[a,b,*]

[a] Center for Ecological Research, Northeast Forestry University, Harbin 150040, China
[b] Key Laboratory of Sustainable Forest Ecosystem Management – Ministry of Education, Northeast Forestry University, Harbin 150040, China

ARTICLE INFO

Keywords:
Interannual variation
Leaf fall
MODIS
Radiometer
Validation

ABSTRACT

Autumn (i.e., leaf-fall) phenology plays an important role in regulating the canopy duration and is often monitored using near-surface and satellite remote sensing techniques, but the measurements have rarely been validated by the ground observation. The objectives of this study were to: (1) evaluate the performance of radiometer-based broadband vegetation index (VI_B) and Moderate Resolution Imaging Spectroradiometer (MODIS) vegetation index (VI_M) in monitoring the autumn phenology of a Chinese temperate deciduous forest with decadal (2008 – 2018) leaf-litterfall measurements, and (2) explore the feasibility of using VI_B to validate the VI_M products for monitoring the autumn phenology. We found that the seasonal and interannual trends of both VI_B and VI_M agreed well with those of the leaf-litterfall (correlation coefficients $r > 0.93$). The broadband normalized difference vegetation index ($NDVI_B$) best tracked the interannual variation in the end-of-season (EOS) among the six metrics of the VI_B investigated, while the MODIS enhanced vegetation index (EVI_M) did so among the six metrics of the VI_M, with the corresponding determination coefficient (R^2) of 0.66 and 0.44 with the EOS estimated by the leaf-litterfall. The EOS estimated by VI_B and VI_M was 0 – 11 d earlier than that by the leaf-litterfall. Comparing the six metrics of VI_M with the corresponding ones of VI_B, the EOS derived from the NDVI had the closest correlation with each other ($R^2 = 0.67$). Conclusively, our study validated the remote-sensed leaf-fall phenology with decadal ground measurements, and suggested that radiometer and MODIS could effectively track the autumn phenology in temperate deciduous forests and the leaf-litterfall collection could be used as a complementary approach.

1. Introduction

Vegetation phenology is an important proxy of climate change (Chen et al., 2019; Cleland et al., 2007; Ge et al., 2015; Körner and Basler, 2010). Variations in phenology markedly influence the carbon and nutrient cycling of terrestrial ecosystems (Estiarte and Peñuelas, 2015; Piao et al., 2007, 2008). Accurately monitoring vegetation phenology is thus crucial to understanding land surface processes and improving carbon cycling models in forest ecosystems under global climate change scenarios (Chen et al., 2016; Richardson et al., 2013a).

Vegetation phenology can be monitored by the ground observation, near-surface and satellite remote sensing, eddy covariance technique, etc. (Cleland et al., 2007; Richardson et al., 2013b); and each method has its advantages and disadvantages (Table 1; Piao et al., 2019). The ground observation records specific phenology events (e.g., budburst, leaf-out, coloration, defoliation) at the individual level and is spatiotemporally dispersed, while the satellite remote sensing approach characterizes spatially-continuous phenology at the regional and global scales (Table 1). However, satellite images [e.g., Moderate Resolution Imaging Spectroradiometer (MODIS), Advanced Very High Resolution Radiometer (AVHRR)] often have a coarse spatial resolution, leading to an incomparable coverage between the ground and satellite measurements (Rodriguez-Galiano et al., 2015; Zhang et al., 2006). Although the Landsat TM/ETM + with a finer spatial resolution can bridge this spatial-scale gap, it is still restricted by its low frequency of the imagery acquisition (Fisher and Mustard, 2007; Melaas et al., 2013). Validating the satellite-based phenology is thus critically required. The near-surface remote sensing, such as phenocam and radiometers with a high sampling frequency and moderate spatial resolution (Table 1), can detect subtle changes in the phenology process and facilitate spatially up-scaling from the individual to landscape level (Gamon, 2015; Richardson et al., 2013b). Therefore, a cross-validation and fusion of multi-methods will improve the accuracy of satellite data and the understanding of phenology at different spatiotemporal scales (Piao et al., 2019).

* Corresponding authors.
E-mail addresses: xcwang_cer@nefu.edu.cn (X. Wang), wangck-cf@nefu.edu.cn (C. Wang).

https://doi.org/10.1016/j.agrformet.2019.107758
Received 2 April 2019; Received in revised form 9 September 2019; Accepted 10 September 2019
Available online 18 September 2019

Table 1
Summary of the positive and negative characteristics of the six methods used for monitoring autumn phenology in the literature.

Characteristics	VO	LF	RR	DC	EC	RS
Directness of method	+ +	+ +	−	+	−	−
Small extraction uncertainty	−	−	+ +	+ +	+	− −
Charactering species phenology	+ +	+	− −	+ +	− −	− −
Charactering canopy phenology	− −	+ +	+ +	+ +	+	+
Spatial up-scaling	− −	+	+	+	+	+ +
Temporal resolution	−	−	+ +	+ +	+	−
Long temporal-scale	−	−	+ +	+	+ +	+ +
Labor and time costs	−	− −	+ +	+ +	+ +	+ +
Set-up costs	+ +	+ +	+	+	− −	− −

Very positive (+ +), positive (+), negative (−) or very negative (− −) characteristics of the visual observation (VO), leaf-litterfall collection (LF), routine radiometer (RR), digital camera (DC), eddy covariance (EC), and satellite remote sensing (RS) methods.

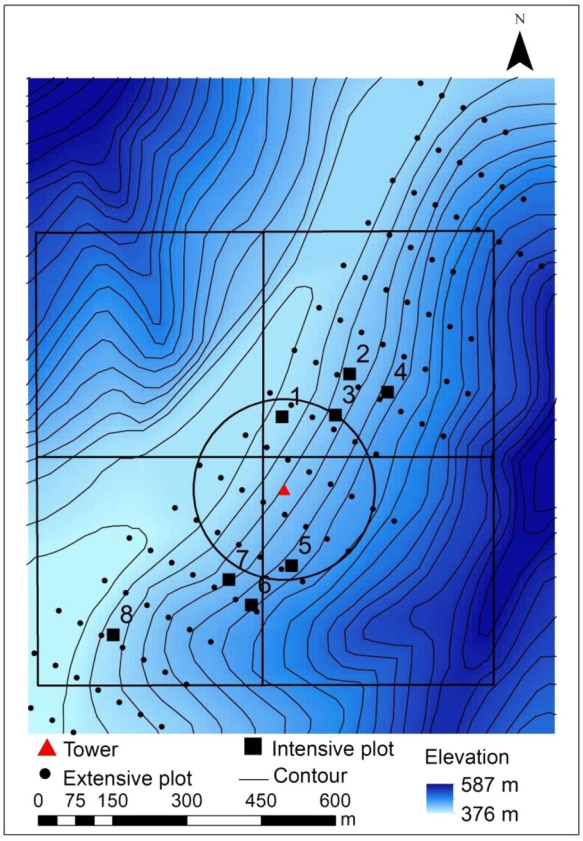

Fig. 1. Contour map and plot distribution around the eddy flux tower at the Maoershan site, northeastern China. The four squares and one circle represent the four pixels of MODIS and the reflective footprint of the radiometers installed on the eddy-flux tower (90% of signal), respectively.

There are many studies focusing on spring phenology and the validation of satellite products with ground observations or near-surface sensors (e.g. Liang et al., 2011; Maignan et al., 2008; Peng et al., 2017a; Studer et al., 2007), which confirm that the spring phenology derived from the ground observation, phenocam, and MODIS products is well-matched (Klosterman et al., 2014; Peng et al., 2017b). However, the autumn phenology has largely been neglected in the global warming studies (Peng et al., 2019; Zohner et al., 2019), probably because of the difficulty of its definition and complex drivers (Diao, 2019; Gallinat et al., 2015; Gill et al., 2015; Keenan and Richardson, 2015; Liu et al., 2016b; Panchen et al., 2015). To date, only a few validations of the satellite products of autumn phenology have been performed with the ground observation or near-surface remote sensing, but no conclusive results have been reached yet. For example, Rodriguez-Galiano et al. (2015) reported that the autumn phenology derived by Medium Resolution Imaging Spectrometer agreed well with that by the visual observation in central European forests, whereas Testa et al. (2018) reported that the leaf-coloration by MODIS matched poorly with that by the visual observation in French deciduous forests. And some studies reported that the date of full leaf coloration by the visual observation closely corresponded to that by MODIS (Liu et al., 2015a; Zhang et al., 2006). Given these discrepancies and the validations were normally based on two- or three-year observations, it is imperative to evaluate the consistency of different methods with long-term data at the site scale (Helman, 2018).

The leaf-litterfall collection, widely applied for estimating net primary productivity (NPP) and leaf area index (LAI) in forest ecosystems (Gower et al., 1999), is less used for monitoring the autumn phenology largely due to its labor intensity and time consumption; however, it directly reflects changes in canopy leaf mass and avoids the subjectivity of the observers in visual observations (Gallinat et al., 2015). Moreover, as a stand-scale observation, it also reduces potential spatial- and species-mismatches between satellite and ground observations (Fisher et al., 2006; Rodriguez-Galiano et al., 2015; Testa et al., 2018). In this study, we applied the leaf-litterfall collection method to obtain a decadal (2008 – 2018) record of the autumn phenology of a temperate mixed deciduous forest in northeastern China. Our objectives were to: (1) evaluate the performance of radiometer-based broadband vegetation index (VI_B) and Moderate Resolution Imaging Spectroradiometer (MODIS) vegetation index (VI_M) in monitoring the autumn phenology of the forest with decadal leaf-litterfall measurements, and (2) explore the feasibility of using VI_B to validate the VI_M products for monitoring the autumn phenology.

2. Materials and methods

2.1. Site description

The study was conducted at the Maoershan Forest Ecosystem Research Station of Northeast Forestry University, Heilongjiang Province, Northeast China (45°24′N, 127°40′E, 400 m a.s.l.). The climate is a continental monsoon climate. The mean (2006 – 2017) annual air temperature was 2.2 °C. The mean annual rainfall was 591 mm (Wang et al., 2019). A 48-m high eddy-flux tower was established on the northwest-facing (~296 °) slope, with an average slope of ~9 ° (Fig. 1; Wang et al., 2016). The stand is a temperate deciduous forest with a 18 – 20 m high canopy, which is dominated by *Ulmus japonica, Fraxinus mandshurica, Betula platyphylla, Populus davidiana*, etc. The mean (2008 – 2018) maximum LAI estimated by the litterfall collection was 6.2 m^2 m^{-2} (Liu et al., unpublished data).

2.2. Data collection

2.2.1. Leaf-litterfall collection and leaf mass estimation

Five 1-m^2 litter traps were randomly installed in each of eight 20 m × 30 m intensive plots distributed within the range of 100 – 500 m around the eddy-flux tower (Fig. 1). We periodically collected the litterfall, i.e., monthly before July, semimonthly in August, and

Table 2
Equations for calculating various vegetation indices.

Vegetation index	Equation	Reference
Normalized difference vegetation index (NDVI)	$NDVI = \frac{r_{NIR} - r_{PAR}}{r_{NIR} + r_{PAR}}$	(Huemmrich et al., 1999; Rouse et al., 1974)
Enhanced vegetation index (EVI)	$EVI = \frac{2.5 \times (r_{NIR} - r_{PAR})}{r_{NIR} + 2.4 \times r_{PAR} + 1}$	(Jiang et al., 2008; Rocha and Shaver, 2009)
Simple ratio of the albedo of near-infrared to photosynthetically active radiation (SR)	$SR = \frac{r_{NIR}}{r_{PAR}}$	(Rouse et al., 1974; Wang et al., 2008)
Wide dynamic range vegetation index (WDRVI)	$WDRVI = \frac{0.1 \times r_{NIR} - r_{PAR}}{0.1 \times r_{NIR} + r_{PAR}}$	(Gitelson, 2004)
Global environmental monitoring index (GEMI)	$GEMI = \eta(1 - 0.25 \times \eta) - \frac{r_{PAR} - 0.125}{1 - r_{PAR}}$ $\eta = \frac{2 \times (r_{NIR}^2 - r_{PAR}^2) + 1.5 \times r_{NIR} + 0.5 \times r_{PAR}}{r_{NIR} + r_{PAR} + 0.5}$	(Pinty and Verstraete, 1992)
Soil-adjusted vegetation index (SAVI)	$SAVI = \frac{1.5 \times (r_{NIR} - r_{PAR})}{r_{NIR} + r_{PAR} + 1}$	(Huete, 1988)

The r_{PAR} and r_{NIR} are the albedos of photosynthetically active radiation (PAR) and near-infrared radiation (NIR), respectively.

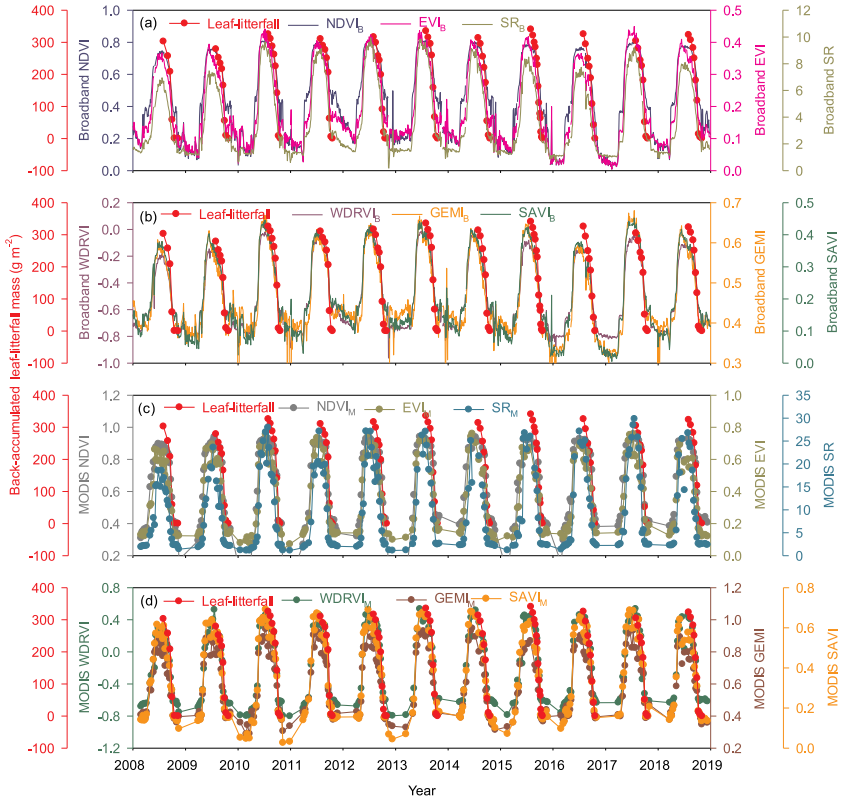

Fig. 2. Temporal dynamics in the leaf-litterfall mass (back-accumulated), broadband and MODIS vegetation indices (VIs) during the period between 2008 and 2018. NDVI: normalized difference vegetation index, EVI: enhanced vegetation index, SR: simple ratio of the albedo of near-infrared to photosynthetically active (or red band) radiation, WDRVI: wide dynamic range vegetation index, GEMI: global environmental monitoring index, SAVI: soil-adjusted vegetation index. The subscripts B and M represent the broadband and MODIS VIs, respectively.

every 10 days in the autumn (September and October) from 2008 to 2018. To explore the effect of collection frequency on the estimation of the end-of-season (EOS), we emptied the litter traps every 5 days in the autumn of 2015. The litterfall was sorted into leaves, twigs and other tissues, oven-dried at 70 °C for 48 h, and weighed for the dry mass (0.01 g). Then the leaf mass in the canopy was back-accumulated by leaf-fall mass for each collection (Liu et al., 2015b).

We assumed that the leaf mass loss during the leaf senescence and decomposition before litter collection (Wang et al., 2019) would not significantly affect the EOS extraction because it only used the relative change rate of the leaf mass. To verify whether the eight intensive plots well represented the species composition for comparing with the MODIS pixels (Helman, 2018; Rodriguez-Galiano et al., 2015), we surveyed additional 106 extensive plots and found roughly consistent species composition (*U. japonica* 21%, *F. mandshurica* 16%, and *B. platyphylla* 15% of basal area for the intensive plots versus 21%, 12%, 14%, respectively, for the extensive plots). Additionally, the intensive plots also had a reasonable spatial representativeness (i.e., terrain, slope, and location) for the MODIS pixels (Fig. 1).

2.2.2. Radiation measurements and calculation of broadband vegetation index

The incoming solar (SOLR, 300 – 2800 nm, W m^{-2}) and long-wave radiations (4.5 – 42 μm) were measured by a net radiometer (CNR1 or CNR4, Kipp & Zonen, the Netherlands) installed at the 48-m height of the eddy-flux tower. We also measured the incident and reflected

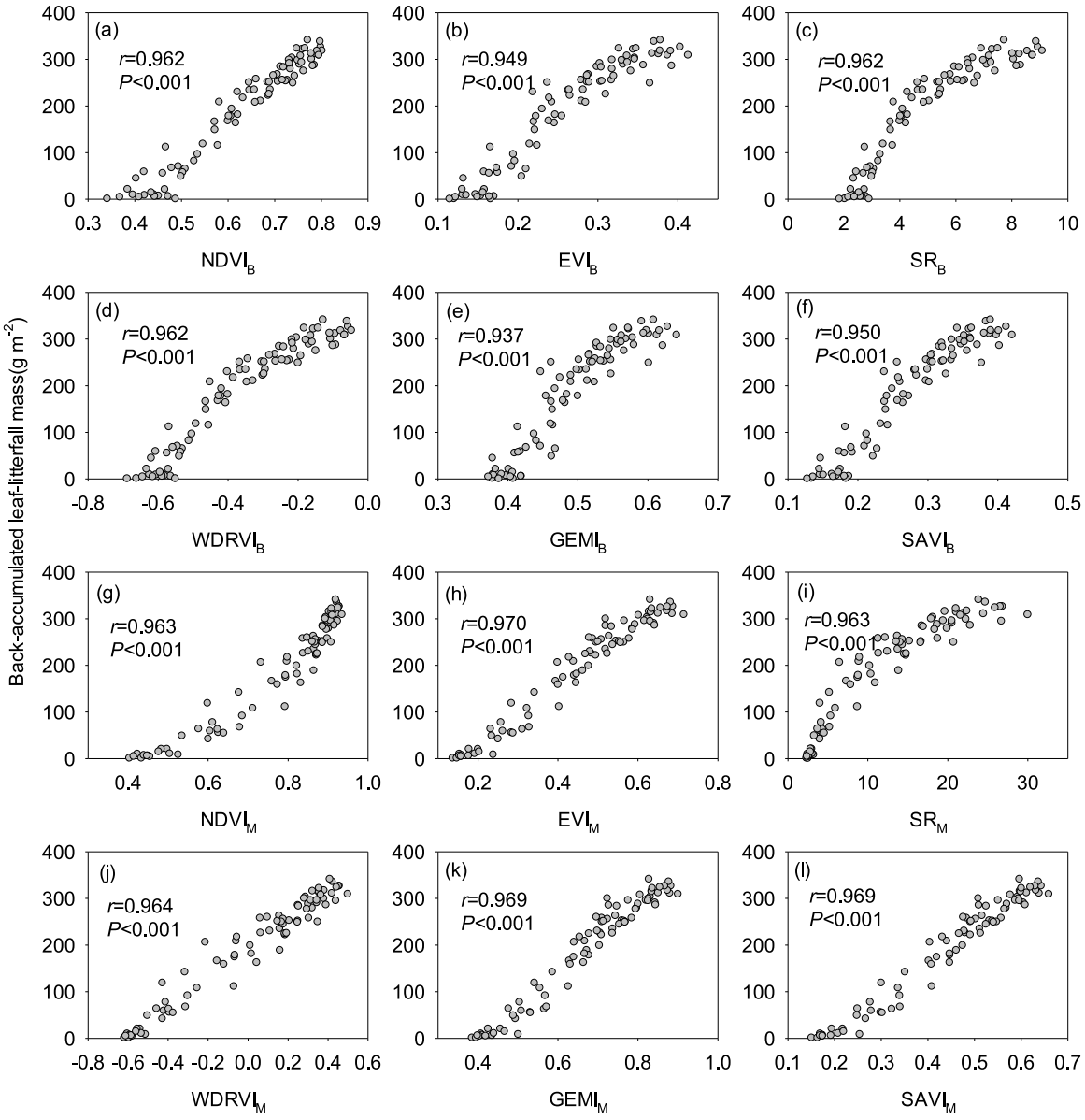

Fig. 3. Spearman's rank correlation between vegetation indices and back-accumulated leaf-litterfall mass.

photosynthetically active radiation (PAR, 400 – 700 nm, μmol $m^{-2} s^{-1}$) by a pair of PQS1 or PARLITE sensors (Kipp & Zonen, the Netherlands). All the radiation data were sampled every 5 s, averaged every 30 min, and stored in a CR1000 datalogger (Campbell, Scientific, Inc., Logan, UT, USA).

Six VI_B were calculated with different combinations of the albedo of PAR (r_{PAR}) and the near-infrared radiation (r_{NIR}) (Table 2), including the normalized difference vegetation index (NDVI) (Huemmrich et al., 1999; Rouse et al., 1974), the enhanced vegetation index (EVI) (Jiang et al., 2008; Rocha and Shaver, 2009), the simple ratio of r_{NIR} to r_{PAR} (SR) (Rouse et al., 1974; Wang et al., 2008), the wide dynamic range vegetation index (WDRVI) (Gitelson, 2004), the global environment monitoring index (GEMI) (Pinty and Verstraete, 1992), and the soil-adjusted vegetation index (SAVI) (Huete, 1988).

The PAR was converted to the energy flux density with the conversion coefficients [the incident coefficient 0.2195 J μmol $photon^{-1}$, the reflected coefficient 0.2072 J μmol $photon^{-1}$(Ross and Sulev, 2000)], and then the near-infrared radiation (NIR) was calculated by the difference between of SOLR and PAR. The r_{PAR} and r_{NIR} were calculated as (Liu et al., 2019):

$$r_{PAR} = \frac{PAR_{out}}{PAR_{in}} \quad (1)$$

$$r_{NIR} = \frac{SOLR_{out} - PAR_{out}}{SOLR_{in} - PAR_{in}} \quad (2)$$

where PAR_{out}, PAR_{in}, $SOLR_{out}$, and $SOLR_{in}$ are the reflected and incident PAR and solar radiation, respectively.

The noises of VI_B time series were smoothed by a moving window approach that assigned the 50th percentile of the values around noon (10:00 – 14:00 local time) within a 3-d window to the center day

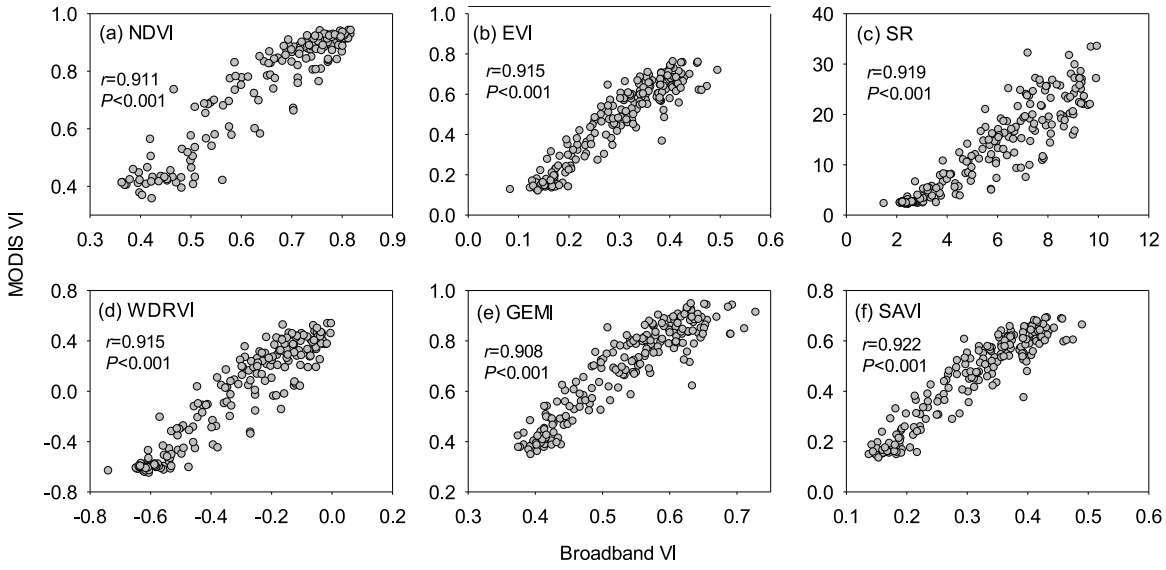

Fig. 4. Spearman's rank correlation between 8-d MODIS and the corresponding broadband vegetation indices (VIs).

(Hufkens et al., 2012; Liu et al., 2018).

2.2.3. MODIS products

A product of 500-m surface reflectance data from Terra instrument (MOD09A1) was obtained from ORNL DAAC (DAAC, 2018a; Vermote, 2015), which was an 8-d composite by selecting observations with favorable viewing geometry and minimal cloud cover. The daily nadir bidirectional reflectance distribution function-adjusted reflectance product (MCD43A4) (DAAC, 2018b; Schaaf and Wang, 2015) was also used. Six VI_M (i.e., $NDVI_M$, EVI_M, SR_M, $WDRVI_M$, $GEMI_M$, and $SAVI_M$) were calculated by the equations in Table 2 using band 1 (red, 620 – 670 nm) and 2 (NIR, 841 – 876 nm). The reflectance of band 3 (blue, 459 – 479 nm) was added to calculate the EVI_M as:

$$EVI_M = \frac{2.5(r_{NIR} - r_{red})}{r_{NIR} + 6r_{red} - 7.5r_{blue} + 1} \quad (3)$$

where r_{NIR}, r_{red}, and r_{blue} are the reflectance of near-infrared, red, and blue bands, respectively. Because our eddy-flux tower was located at the edge of one MODIS pixel (Fig. 1), we used the mean value of the four pixels around the tower for inter-comparisons with other methods.

2.3. Phenophase extraction

A simple logistic model was used to fit the time series of the back-accumulated leaf-litterfall and all the vegetation indices (VIs). The EOS was defined as the date corresponding to the maximum of the first derivative of the fitted curve [f(t) in Eq. (4)], representing the most-rapidly decreasing date (i.e., the leaf-fall peak) (Fisher et al., 2006).

$$f(t) = a - \frac{b}{1 + e^{(c-t)/d}} \quad (4)$$

where t is the day of year (DOY), a is the maximum VI in autumn, b is the VI amplitude; c and d represent the inflection point and the decrease rate of the VI, respectively. The uncertainty of the EOS estimate was evaluated by the average width of inner 95% confidence intervals (Klosterman et al., 2014).

2.4. Statistic analysis

The spearman's rank correlation was used to evaluate the synchronism of the time series between methods (Delpierre et al., 2017). The least-square linear regression and the determination of coefficient (R^2) were used to assess the consistency of interannual trends of the EOS estimated by different methods. The mean bias and mean absolute deviation (MAD) were calculated for the EOS estimated by various methods as:

$$\text{mean bias} = \frac{\sum_{i=1}^{N} (EOS_i - EOS_{refi})}{N} \quad (5)$$

$$MAD = \frac{\sum_{i=1}^{N} |EOS_i - EOS_{refi}|}{N} \quad (6)$$

where N is the number of years (11 in this study); EOS_i and EOS_{refi} represent the EOS estimated by a specific method and the reference in the ith year, respectively. The EOS derived by the leaf-litterfall was used as the reference when comparing the VI_B and VI_M with the leaf-litterfall, whereas that by VI_B was used as the reference when comparing VI_M with VI_B. The positive (negative) bias indicated that the EOS was later (earlier) than the reference. All statistical analyses were performed by SPSS 19.0 software.

3. Results

3.1. Temporal dynamics in leaf-litterfall mass and vegetation indices

The temporal dynamics in the leaf-litterfall, VI_B and VI_M were highly consistent (Fig. 2), with all the correlation coefficients (r) between the VI_B or VI_M and the leaf-litterfall mass being greater than 0.93 (Fig. 3). The r between the VI_M and VI_B varied from 0.90 to 0.93, with the VI_B amplitude being slightly less than the VI_M amplitude (Fig. 4).

3.2. Comparisons of EOS estimated by near-surface, MODIS remote sensing and leaf-litterfall methods

The interannual ranges of the EOS estimated by the leaf-litterfall,

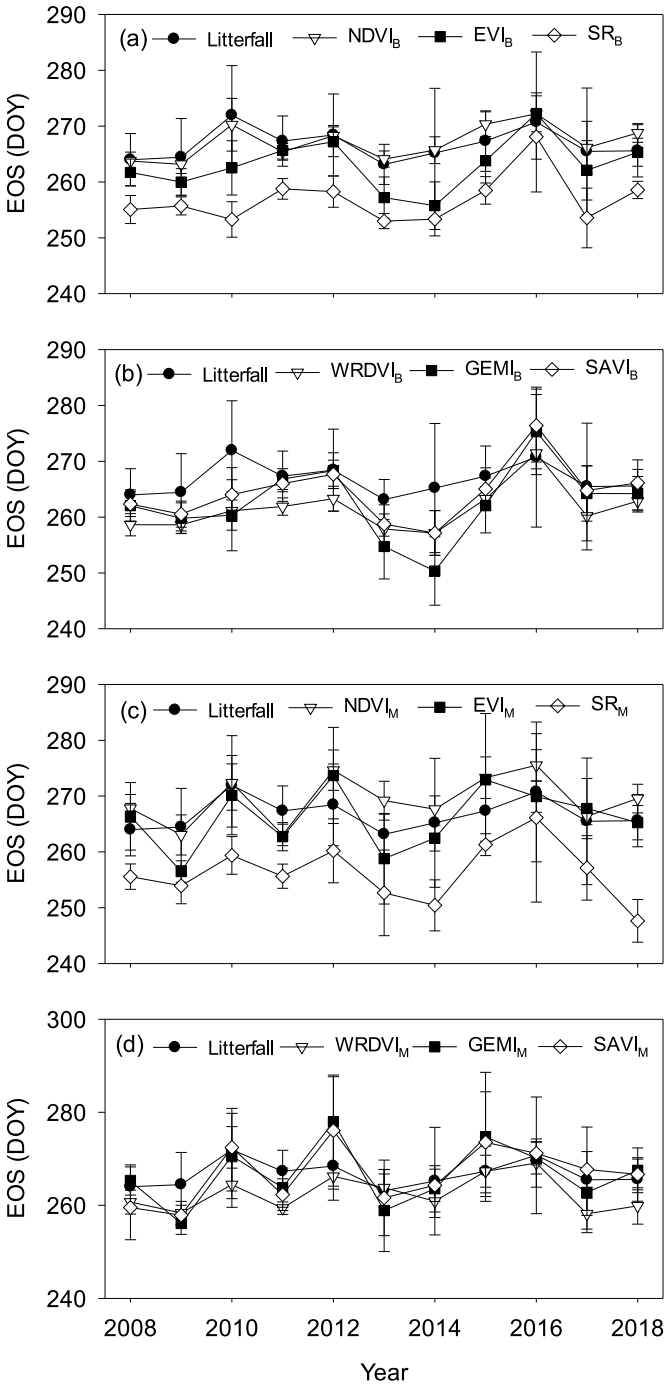

Fig. 5. Interannual fluctuations in the end-of-season (EOS) derived from leaf-litterfall, broadband and 8-d MODIS vegetation indices during the period between 2008 and 2018. The error bars indicate 95% confidence intervals of the EOS estimates.

VI_B, and VI_M were 9 d, 9 ($NDVI_B$) – 25 ($GEMI_B$) d, and 11 ($WDRVI_M$) – 22 ($GEMI_M$) d, respectively (Fig. 5). Although there were no significant delaying trends for any method, most of the EOS derived from the leaf-litterfall and VIs in 2010, 2012 and 2016 were later than those in the other years during 2008 – 2018 (Fig. 5). The R^2 of VI_B and VI_M with leaf-litterfall ranged from 0.15 – 0.66 and 0.34 – 0.44, respectively. The mean bias and MAD of the EOS derived from the six VI_B were −10 – 0 d and 1 – 10 d, respectively; and those from the VI_M were −11 – 2 d and 3 – 11 d, respectively. For the near-surface method, the $NDVI_B$ had the highest R^2 (0.66, Fig. 7a) and least mean bias (0 d, Fig. 7b) and MAD (1 d, Fig. 7c). For the MODIS method, the EOS estimated by the six VI_M were all significantly correlated with that by leaf-litterfall, of which the EVI_M had the highest R^2 (0.44) and relatively lower bias and MAD (−1 and 4 d, respectively, Fig. 7). The most-used $NDVI_M$ performed moderately well (R^2 = 0.34) with an intermediate bias of 2 d and the lowest MAD of 3 d.

3.3. Consistency of EOS estimated by near-surface and MODIS remote sensing methods

The EOS derived from two of the six VI_M ($NDVI_M$ and $WDRVI_M$) was significantly correlated with that from the counterparts of VI_B (Fig. 8), with the R^2 being 0.67 and 0.38, respectively (Fig. 9a). The EOS derived from VI_M was −2 (SR_M) – 4 d ($GEMI_M$) later than that from VI_B (Fig. 9b); and the MAD between them varied from 3 d ($NDVI_M$) to 7 d ($GEMI_M$). Among the VIs investigated, the $NDVI_B$ and $NDVI_M$ had the highest R^2 (0.67) when deriving the EOS, of which the regression had a moderate bias and MAD (2 and 3 d, respectively) in the EOS (Fig. 9).

4. Discussion

4.1. Comparing near-surface and MODIS remote sensing methods for monitoring autumn phenology

The close correlation of the seasonal and interannual trends between VI_M and VI_B (Figs. 2 and 4) displays the reliability of MODIS products for monitoring the autumn phenology at our temperate forest site. Similarly, the seasonal courses of VI_B agreed with the satellite data at other forest sites (Huemmrich et al., 1999; Wilson and Meyers, 2007). We also found that the EOS derived by $NDVI_B$ had the closest correlation with that by $NDVI_M$ among the six VI_B investigated (Figs. 8 and 9), consistent with previous studies on spring phenology (Balzarolo et al., 2016). Accordingly, we recommend using $NDVI_B$ for validating MODIS phenology products.

The EOS estimated by VI_M was 2 – 4 d later than that by VI_B (Fig. 4). These variations in EOS estimated by different methods mainly resulted from the features of remote sensors (e.g., spectral bandwidth, view zenith angle, frequency of data acquisition). For example, the spectral band of routine radiometers is composed of broadband NIR and PAR, while the MODIS sensors have much finer spectral resolutions. VI_B reflects canopy greenness, while VI_M is associated with leaf photosynthesis (Balzarolo et al., 2016). These differences may lead to the divergence in the EOS derived from VI_B and VI_M. Moreover, the view zenith angle of MODIS sensors changes with seasons, which likely alters the viewing area even for the same pixel, and thus affects the EOS estimates (Helman, 2018). Although the temporal resolution of MODIS may have little effect on the phenological estimates (Fig. A1; Liang et al., 2014; White et al., 2014; Zhang et al., 2009), high frequency of satellite data might reveal more details of the phenological processes (Liang et al., 2014).

Additionally, the spatial-resolution mismatch between the two methods also affects the comparability between VI_B and VI_M. For example, our radiometers were mounted at 48 m above the ground surface (i.e., ~ 28 m above the canopy), of which the footprint (9.8×10^4 m^2) was only one-tenth of the area of the four MODIS pixels (4×500 m $\times$ 500 m = 1.0×10^6 m^2). Such spatial mismatch could be worse if the radiometers are installed in a lower position.

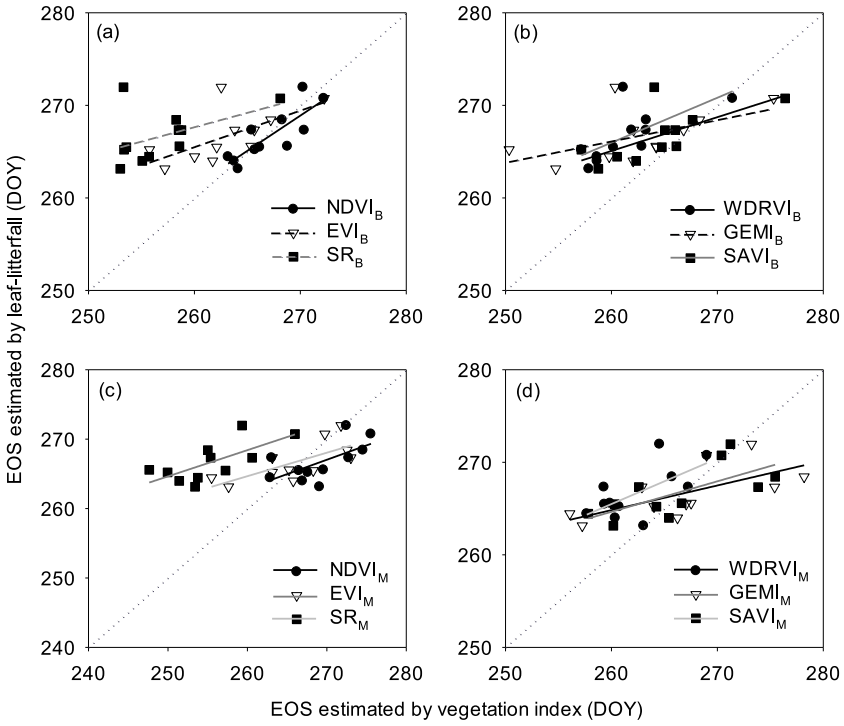

Fig. 6. Relationships between the end-of-season (EOS) estimated by vegetation indices and that by leaf-litterfall. The solid and dash lines represent significant and non-significant regressions, respectively. The dotted diagonal line is the 1:1 line.

Fisher et al. (2006) reported that the difference in the spring phenology within one pixel (< 500 m distance) could reach 10 – 14 d in southern New England, USA. However, our results showed that most of the standard deviations of the EOS estimated from the four MODIS pixels were 1 – 2 d (Table A1), which implies that the spatial variation in EOS at a finer resolution can be reduced by averaging it in a larger area (Peng et al., 2017c).

Currently, several near-surface sensors are applicable for monitoring vegetation phenology and validating MODIS products, such as routine radiometers (Balzarolo et al., 2016), phenocam (Brown et al., 2017; D'Odorico et al., 2015; Liu et al., 2017), etc. As an ancillary equipment of eddy-flux towers, the radiometer has the advantage for validating MODIS phenology at a longer temporal scale (Balzarolo et al., 2016), because the FLUXNET has operated ~10 years earlier than the PhenoCam network (Baldocchi et al., 2001). Additionally, gross primary production and net ecosystem exchange measured by the eddy covariance method are often used as a proxy of the "functional phenology" (Liu et al., 2018), which might be essentially different from the "optical phenology" of VIs. Collectively, the VI$_B$ can complement the satellite data for monitoring autumn phenology (Balzarolo et al., 2016).

4.2. Validating the autumn phenology derived from near-surface and MODIS remote sensing with leaf-litterfall collection

To our best knowledge, our study validated the leaf-fall phenology derived from remote sensing with decadal stand-level ground measurements for the first time. We found that the seasonal patterns and EOSs derived from VI$_B$ and VI$_M$ were generally consistent with those from the leaf-litterfall (Fig. 2) in spite of the ~9 d interannual range of the EOS derived from the litterfall (Fig. 5). This finding demonstrates that VI$_B$ and VI$_M$ can effectively monitor the interannual change of the leaf-fall phenology in temperate deciduous forests. However, several issues need to be addressed in order to improve the consistency of different methods for monitoring the autumn phenology.

First, which VI metric should be used to present the interannual variation in autumn phenology? There are no conclusive answer yet, maybe depending on species or plant functional types (Helman, 2018) or the physiological meanings reflected by different VIs (Mariën et al., 2019). For example, EVI$_B$ is more suitable for grassland, whereas WDRVI$_B$ is better for cropland (Balzarolo et al., 2016; Rocha and Shaver, 2009). Testa et al. (2018) argued that WDRVI$_M$ and EVI$_M$ were the best indicators of initial and advanced yellowing, respectively, by ground visual observations in French deciduous forests; however, the performances of all the VI$_M$ tested were poor (R^2 < 0.27) across the ~60-d ranges of autumn phenology, primarily due to the spatial mismatch and large uncertainty of the EOS estimation (Rodriguez-Galiano et al., 2015; Testa et al., 2018). In our temperate deciduous forest, NDVI$_B$ and EVI$_M$ best reflected the decadal fluctuation of the EOS among the VIs investigated (with highest R^2 against the leaf-litterfall; Figs. 5–7). Also, NDVI$_B$ is the most-used broadband metric and the optimal proxy for predicting canopy LAI change in autumn among the four VI$_B$ (Liu et al., 2016a). However, given the low MAD (Fig. 7c), using NDVI$_M$ may not be discouraged in spite of the moderate R^2. The different performances between VI$_B$ and VI$_M$ may be related to our small interannual range of EOS (9 d, Fig. 5), their spectral resolution and spatial scales.

Second, how to deal with the spatial representativeness for each method? For ground observation, up-scaling from the individual- to stand-level is indispensable for the cross-validation and fusion of multiple-scale data of phenology (Piao et al., 2019). Directly using the average phenology of various species to represent the whole stand

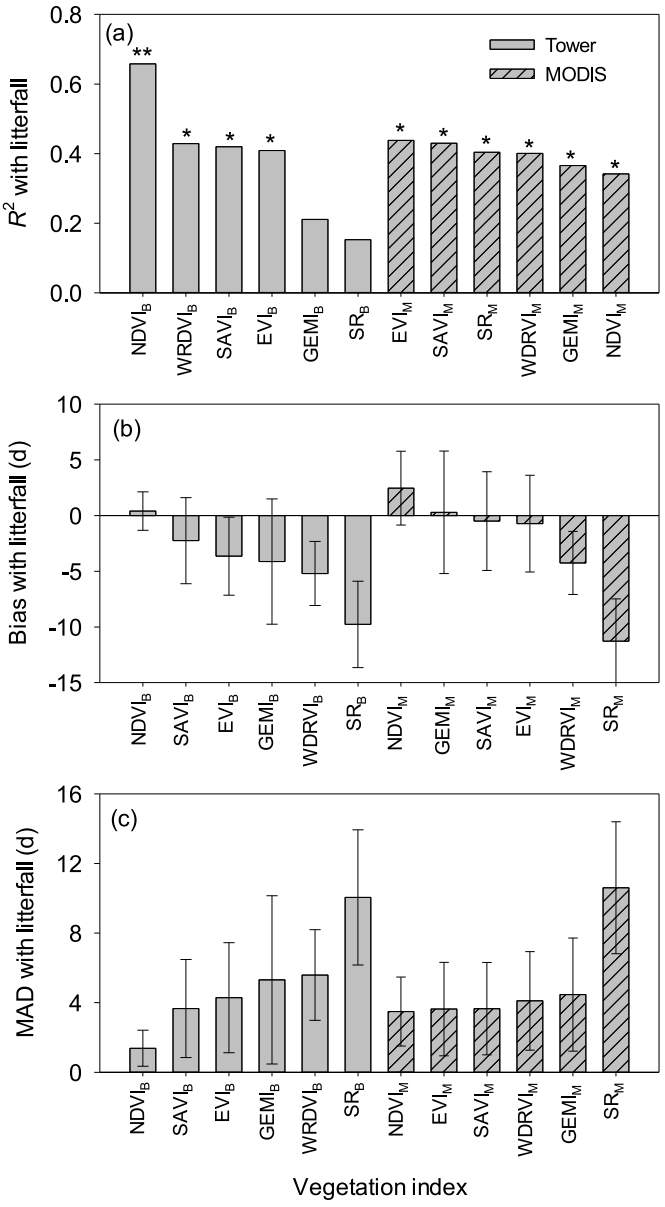

Fig. 7. The determination coefficients (R^2) of the regression equations, mean bias and mean absolute deviation (MAD) of the end-of-season (EOS) derived from broadband or MODIS vegetation indices against that from leaf-litterfall. * and ** indicate the significant correlation at $\alpha = 0.05$ and $\alpha = 0.01$ levels, respectively. The positive (negative) values of biases indicate that the EOS is later (earlier) than the reference. The error bars represent the standard deviations of the bias or MAD across the period between 2008 and 2018.

(Diao, 2019; Rodriguez-Galiano et al., 2015) can introduce a greater uncertainty than does using the phenology of the dominant species or calculating the weighted average based on the basal area of species composition (White et al., 2014). Sometimes it is difficult to determine the dominant tree species in natural mixed forests, which may result in uncertainties in validating the remote-sensed phenology (Rodriguez-Galiano et al., 2015). On the other hand, the weighted average approach underlyingly hypothesizes that the ratio of leaf area to basal area is equal for various species, which may also introduce uncertainties, because the allometry of leaf biomass against tree diameter (Wang, 2006) and/or leaf mass per area (Poorter et al., 2009) normally vary with tree species. The stand-scale litterfall collection (the eight intensive plots distributed over different terrains) effectively reduced the spatial mismatches between methods (Table 1, Fig. 1). Further interpretation of vegetation phenology at different spatial scales can be made with automated unmanned aerial vehicles (Berra et al., 2019; Klosterman et al., 2018; Piao et al., 2019).

Third, how to define the absolute date of autumn penology for each method? The definitions of EOS for the ground observation [e.g., 10%, 50%, or 90% leaf coloration; 50% or 100% leaf-fall, etc. (Gill et al., 2015)] and the methods for EOS extraction with near-surface and satellite remote sensing techniques [the extreme point or mid-point (Helman, 2018), the breakpoint analysis (Mariën et al., 2019)] vary widely in the literature. The absolute dates of the EOS estimated by VI_B and VI_M averaged 0 – 11 d earlier than that by the leaf-litterfall at our site (Fig. 7b). Similarly, the midpoint date of EVI_M was 10 d earlier than the 50% leaf-fall date across Ireland (Donnelly et al., 2018); however, the minimum of EVI_M was ~13 d later than the full leaf-fall date in the Hubbard Brook Forest (Zhang et al., 2006). The earlier EOS derived by VIs may primarily result from the complex mechanisms of leaf senescence and extrinsic features (Maignan et al., 2008; Soudani et al., 2012; Testa et al., 2018). The VIs are sensitive to leaf chlorophyll and water regimes (Mariën et al., 2019; Zhang et al., 2006), thus the leaf fall commonly lags behind coloration (Mariën et al., 2019). And the duration of colored-leaves retaining on the canopy before falling may be related to the meteorological factors (e.g. wind speed and temperature), and thus change from year to year. Such differences in the extrinsic features increase the divergence of autumn phenology derived from different methods. Moreover, the uncertainty of visual record introduced by the subjectivity of the observers is difficult to assess (Peltoniemi et al., 2018; Piao et al., 2019). In contrast, regular leaf-litterfall collection can quantify the leaf-fall rhythm at the stand level and distinguish various species phenology at the individual level by sorting leaf-litterfall by tree species, which substantially reduces the biases associated with the up-scaling and subjectivity. Considering that the litterfall collection is also a common method in other ecological studies (e.g., estimating LAI, components of NPP, and nutrient cycling), it has a broad prospect for deriving leaf-fall phenology.

Finally, how frequently should the litterfall be collected to quantify the leaf-fall phenology? Using the litterfall data with a 5-d interval in the autumn of 2015, we found that the estimated EOS was nearly the same as that with a 10-d interval in the same year (267 ± 5 d vs. 266 ± 6 d, $R^2 > 0.99$). In fact, a 10-d interval of litterfall collection is commonly used to reduce the litter mass loss due to leaching or decomposition in other ecological studies (Wang et al., 2019). Therefore, we recommend a 10-d frequency of leaf-litterfall collection to balance labor/ time costs and accuracy in monitoring autumn phenology.

5. Conclusions

We assessed the performance of near-surface and MODIS remote sensing methods for characterizing the long-term temporal variations in the autumn phenology of a temperate deciduous forest with the leaf-litterfall collection method. All the VIs investigated had consistent temporal patterns with the back-accumulated leaf-litterfall, of which $NDVI_B$ and EVI_M best tracked the interannual trend of the EOS. The EOS estimated by VIs was 0 – 11 d earlier than that by the leaf-litterfall, which could be largely attributed to the different biophysical meanings between VIs and leaf-fall. Our findings supported the application of radiometer and MODIS to monitor seasonal and interannual changes in

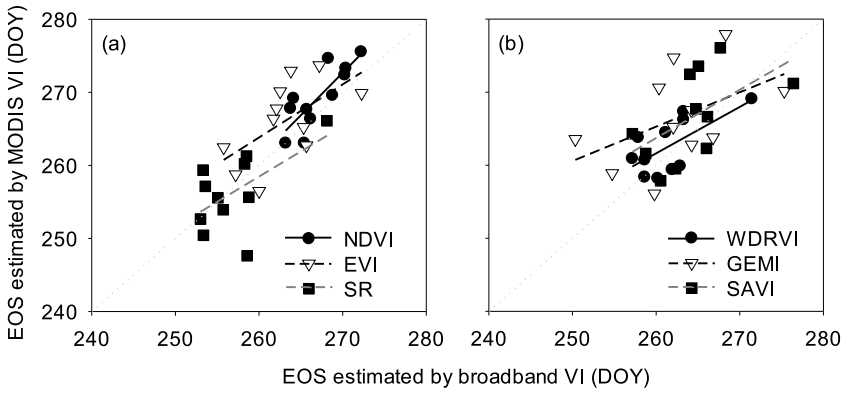

Fig. 8. Relationships between the end-of-season (EOS) estimated by broadband and MODIS vegetation indices. The solid and dash lines represent significant and non-significant regressions, respectively. The dotted diagonal line is the 1:1 line.

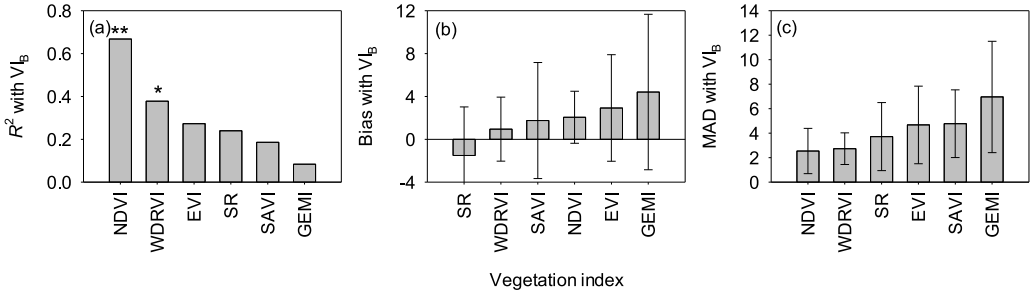

Fig. 9. The determination coefficients (R^2) of the regression equations, mean bias and mean absolute deviation (MAD) of the end-of-season (EOS) derived by MODIS vegetation indices (VIs) against that by the corresponding broadband VIs. * and ** indicate the significant correlation at $\alpha = 0.05$ and $\alpha = 0.01$ levels, respectively.

the autumn phenology in temperate deciduous forests, and the leaf-litterfall collection method could be used as a complementary approach to understand the autumn phenology.

Acknowledgments

This work was supported by the National Science and Technology Support Program of China (2011BAD37B01), the Fundamental Research Funds for the Central Universities (2572019CP07), the Natural Science Foundation of Heilongjiang Province of China (QC2017010), and the Program for Changjiang Scholars and Innovative Research Team in University (IRT_15R09). We thank the two anonymous reviewers and the editor for their valuable comments on the manuscript. We are grateful to Guangdong Cao, Jing Wang, Haiyan Zhang, Yingchi Li, Xiaofeng Sun, Linfeng Zhang for their help on processing the litterfall. The Maoershan Forest Ecosystem Research Station provided field logistic support.

Supplementary materials

Supplementary material associated with this article can be found, in the online version, at doi:10.1016/j.agrformet.2019.107758.

References

Baldocchi, D., Falge, E., Gu, L., Olson, R., Hollinger, D., Running, S., Anthoni, P., Bernhofer, C., Davis, K., Evans, R., 2001. FLUXNET: a new tool to study the temporal and spatial variability of ecosystem-scale carbon dioxide, water vapor, and energy flux densities. Bull. Am. Meteorol. Soc. 82, 2415–2434. https://doi.org/10.1175/1520-0477(2001)082<2415:FANTTS>2.3.CO;2.

Balzarolo, M., Vicca, S., Nguy-Robertson, A.L., Bonal, D., Elbers, J.A., Fu, Y.H., Grünwald, T., Horemans, J.A., Papale, D., Peñuelas, J., 2016. Matching the phenology of net ecosystem exchange and vegetation indices estimated with MODIS and FLUXNET in-situ observations. Remote Sens. Environ. 174, 290–300. https://doi.org/10.1016/j.rse.2015.12.017.

Berra, E.F., Gaulton, R., Barr, S., 2019. Assessing spring phenology of a temperate woodland: a multiscale comparison of ground, unmanned aerial vehicle and Landsat satellite observations. Remote Sens. Environ. 223, 229–242. https://doi.org/10.1016/j.rse.2019.01.010.

Brown, L.A., Dash, J., Ogutu, B.O., Richardson, A.D., 2017. On the relationship between continuous measures of canopy greenness derived using near-surface remote sensing and satellite-derived vegetation products. Agric. For. Meteorol. 247, 280–292. https://doi.org/10.1016/j.agrformet.2017.08.012.

Chen, L., Huang, J.-.G., Ma, Q., Hänninen, H., Tremblay, F., Bergeron, Y., 2019. Long-term changes in the impacts of global warming on leaf phenology of four temperate tree species. Global Change Biol. 25, 997–1004. https://doi.org/10.1111/gcb.14496.

Chen, M., Melaas, E.K., Gray, J.M., Friedl, M.A., Richardson, A.D., 2016. Improving the seasonal-deciduous spring phenology submodel in the Community Land Model 4.5: impacts on carbon and water cycling under future climate scenarios. Global Change Biol. 22, 3675–3688. https://doi.org/10.1111/gcb.13326.

Cleland, E.E., Chuine, I., Menzel, A., Mooney, H.A., Schwartz, M.D., 2007. Shifting plant phenology in response to global change. Trends Ecol. Evol. 22, 357–365. https://doi.org/10.1016/j.tree.2007.04.003.

D'Odorico, P., Gonsamo, A., Gough, C.M., Bohrer, G., Morison, J., Wilkinson, M., Hanson, P.J., Gianelle, D., Fuentes, J.D., Buchmann, N., 2015. The match and mismatch between photosynthesis and land surface phenology of deciduous forests. Agric. For. Meteorol. 214, 25–38. https://doi.org/10.1016/j.agrformet.2015.07.005.

DAAC, O., 2018. MODIS and VIIRS Land Products Global Subsetting and Visualization Tool. ORNL DAAC, Oak Ridge, Tennessee, USA. https://doi.org/10.3334/ORNLDAAC/1379. Accessed June 06, 2019. Subset obtained for MOD09A1 product at 45.42N,127.67E, time period: 2000-02-18 to 2019-05-17, and subset size: 2.5×2.5km.

DAAC, O., 2018. MODIS and VIIRS Land Products Global Subsetting and Visualization Tool. ORNL DAAC, Oak Ridge, Tennessee, USA. https://doi.org/10.3334/ORNLDAAC/1379. Accessed June 07, 2019. Subset obtained for MCD43A4 product at 45.42N,127.67E, time period: 2000-02-24 to 2019-05-24, and subset size: 2.5×2.5km.

Delpierre, N., Guillemot, J., Dufrêne, E., Cecchini, S., Nicolas, M., 2017. Tree phenological ranks repeat from year to year and correlate with growth in temperate deciduous forests. Agric. For. Meteorol. 234, 1–10. https://doi.org/10.1016/j.agrformet.2016.12.008.

Diao, C., 2019. Complex network-based time series remote sensing model in monitoring the fall foliage transition date for peak coloration. Remote Sens. Environ. 229, 179–192. https://doi.org/10.1016/j.rse.2019.05.003.

Donnelly, A., Liu, L., Zhang, X., Winglerd, A., 2018. Autumn leaf phenology: discrepancies between *in situ* observations and satellite data at urban and rural sites. Int. J. Remote Sens. 39, 8129–8150. https://doi.org/10.1080/01431161.2018.1482021.

Estiarte, M., Peñuelas, J., 2015. Alteration of the phenology of leaf senescence and fall in winter deciduous species by climate change: effects on nutrient proficiency. Global Change Biol. 21, 1005–1017. https://doi.org/10.1111/gcb.12804.

Fisher, J.I., Mustard, J.F., 2007. Cross-scalar satellite phenology from ground, Landsat, and MODIS data. Remote Sens. Environ. 109, 261–273. https://doi.org/10.1016/j.

rse.2007.01.004.
Fisher, J.I., Mustard, J.F., Vadeboncoeur, M.A., 2006. Green leaf phenology at Landsat resolution: scaling from the field to the satellite. Remote Sens. Environ. 100, 265–279. https://doi.org/10.1016/j.rse.2005.10.022.
Gallinat, A.S., Primack, R.B., Wagner, D.L., 2015. Autumn, the neglected season in climate change research. Trends Ecol. Evol. 30, 169–176. https://doi.org/10.1016/j.tree.2015.01.004.
Gamon, J.A., 2015. Reviews and syntheses: optical sampling of the flux tower footprint. Biogeoscience 12, 4509–4523. https://doi.org/10.5194/bg-12-4509-2015.
Ge, Q.S., Wang, H.J., Rutishauser, T., Dai, J.H., 2015. Phenological response to climate change in China: a meta-analysis. Global Change Biol. 21, 265–274. https://doi.org/10.1111/gcb.12648.
Gill, A.L., Gallinat, A.S., Sandersdemott, R., Rigden, A.J., Short, D.G., Mantooth, J.A., Templer, P.H., 2015. Changes in autumn senescence in northern hemisphere deciduous trees: a meta-analysis of autumn phenology studies. Ann. Bot. 116, 875–888. https://doi.org/10.1093/aob/mcv055.
Gitelson, A.A., 2004. Wide dynamic range vegetation index for remote quantification of biophysical characteristics of vegetation. J. Plant Physiol. 161, 165–173. https://doi.org/10.1078/0176-1617-01176.
Gower, S.T., Kucharik, C.J., Norman, J.M., 1999. Direct and indirect estimation of leaf area index, f_{APAR}, and net primary production of terrestrial ecosystems. Remote Sens. Environ. 70, 29–51. https://doi.org/10.1016/S0034-4257(99)00056-5.
Helman, D., 2018. Land surface phenology: what do we really 'see' from space? Sci. Total Environ. 618, 665–673. https://doi.org/10.1016/j.scitotenv.2017.07.237.
Huemmrich, K.F., Black, T.A., Jarvis, P.G., Mccaughey, J.H., Hall, F.G., 1999. High temporal resolution ndvi phenology from micrometeorological radiation sensors. J. Geophys. Res. Atmos. 104, 27935–27944. https://doi.org/10.1029/1999jd900164.
Huete, A.R., 1988. A soil-adjusted vegetation index (SAVI). Remote Sens. Environ. 25, 295–309. https://doi.org/10.1016/0034-4257(88)90106-x.
Hufkens, K., Friedl, M., Sonnentag, O., Braswell, B.H., Milliman, T., Richardson, A.D., 2012. Linking near-surface and satellite remote sensing measurements of deciduous broadleaf forest phenology. Remote Sens. Environ. 117, 307–321. https://doi.org/10.1016/j.rse.2011.10.006.
Jiang, Z., Huete, A.R., Didan, K., Miura, T., 2008. Development of a two-band enhanced vegetation index without a blue band. Remote Sens. Environ. 112, 3833–3845. https://doi.org/10.1016/j.rse.2008.06.006.
Körner, C., Basler, D., 2010. Phenology under global warming. Science 327, 1461–1462. https://doi.org/10.1126/science.1186473.
Keenan, T.F., Richardson, A.D., 2015. The timing of autumn senescence is affected by the timing of spring phenology: implications for predictive models. Global Change Biol. 21, 2634–2641. https://doi.org/10.1111/gcb.12890.
Klosterman, S., Melaas, E., Wang, J.A., Martinez, A., Frederick, S., O'Keefe, J., Orwig, D.A., Wang, Z., Sun, Q., Schaaf, C., Friedl, M., Richardson, A.D., 2018. Fine-scale perspectives on landscape phenology from unmanned aerial vehicle (UAV) photography. Agric. For. Meteorol. 248, 397–407. https://doi.org/10.1016/j.agrformet.2017.10.015.
Klosterman, S.T., Hufkens, K., Gray, J.M., Melaas, E., Sonnentag, O., Lavine, I., Mitchell, L., Norman, R., Friedl, M.A., Richardson, A.D., 2014. Evaluating remote sensing of deciduous forest phenology at multiple spatial scales using PhenoCam imagery. Biogeoscience 11, 4305–4320. https://doi.org/10.5194/bg-11-4305-2014.
Liang, L., Schwartz, M., Wang, Z., Gao, F., B., Schaaf, C., Tan, B., Morisette, J., Zhang, X., 2014. A cross comparison of spatiotemporally enhanced springtime phenological measurements from satellites and ground in a northern U.S. mixed forest. IEEE Trans. Geosci. Remote Sens. 52, 7513–7526. https://doi.org/10.1109/TGRS.2014.2313558.
Liang, L., Schwartz, M.D., Fei, S., 2011. Validating satellite phenology through intensive ground observation and landscape scaling in a mixed seasonal forest. Remote Sens. Environ. 115, 143–157. https://doi.org/10.1016/j.rse.2010.08.013.
Liu, F., Wang, C., Wang, X., 2016a. Monitoring temporal dynamics in leaf area index of the temperate broadleaved deciduous forest in Maoershan region with tower-based radiation measurements. Chin. J. Appl. Ecol. 27, 2409–2419. https://doi.org/10.13287/j.1001-9332.201608.031.
Liu, F., Wang, C., Wang, X., 2018. Application of near-surface remote sensing in monitoring dynamics of forest canopy phenology. Chin. J. Appl. Ecol. 29, 1768–1778. https://doi.org/10.13287/j.1001-9332.201806.016.
Liu, F., Wang, X., Wang, C., 2019. Measuring vegetation phenology with near-surface remote sensing in a temperate deciduous forest: effects of sensor type and deployment. Remote Sens. 11. https://doi.org/10.3390/rs11091063.
Liu, L., Liang, L., Schwartz, M.D., Donnelly, A., Wang, Z., Schaaf, C.B., Liu, L., 2015a. Evaluating the potential of MODIS satellite data to track temporal dynamics of autumn phenology in a temperate mixed forest. Remote Sens. Environ. 160, 156–165. https://doi.org/10.1016/j.rse.2015.01.011.
Liu, Q., Fu, Y.H., Zhu, Z., Liu, Y., Liu, Z., Huang, M., Janssens, I.A., Piao, S., 2016b. Delayed autumn phenology in the Northern Hemisphere is related to change in both climate and spring phenology. Global Change Biol. 22, 3702–3711. https://doi.org/10.1111/gcb.13311.
Liu, Y., Hill, M.J., Zhang, X., Wang, Z., Richardson, A.D., Hufkens, K., Filippa, G., Baldocchi, D.D., Ma, S., Verfaillie, J., Schaaf, C.B., 2017. Using data from Landsat, MODIS, VIIRS and PhenoCams to monitor the phenology of California oak/grass savanna and open grassland across spatial scales. Agric. For. Meteorol. 237-238, 311–325. https://doi.org/10.1016/j.agrformet.2017.02.026.
Liu, Z., Wang, C., Chen, J.M., Wang, X., Jin, G., 2015b. Empirical models for tracing seasonal changes in leaf area index in deciduous broadleaf forests by digital hemispherical photography. For. Ecol. Manage. 351, 67–77. https://doi.org/10.1016/j.foreco.2015.05.005.
Maignan, F., Bréon, F.M., Bacour, C., Demarty, J., Poirson, A., 2008. Interannual vegetation phenology estimates from global AVHRR measurements: comparison with in situ data and applications. Remote Sens. Environ. 112, 496–505. https://doi.org/10.1016/j.rse.2007.05.011.
Mariën, B., Balzarolo, M., Dox, I., Leys, S., Lorène, M.J., Geron, C., Portillo-Estrada, M., AbdElgawad, H., Asard, H., Campioli, M., 2019. Detecting the onset of autumn leaf senescence in deciduous forest trees of the temperate zone. New Phytol. https://doi.org/10.1111/nph.15991.
Melaas, E.K., Friedl, M.A., Zhu, Z., 2013. Detecting interannual variation in deciduous broadleaf forest phenology using Landsat TM/ETM+ data. Remote Sens. Environ. 132, 176–185. https://doi.org/10.1016/j.rse.2013.01.011.
Panchen, Z.A., Primack, R.B., Gallinat, A.S., Nordt, B., Stevens, A.D., Du, Y., Fahey, R., 2015. Substantial variation in leaf senescence times among 1360 temperate woody plant species: implications for phenology and ecosystem processes. Ann. Bot. 116, 865–873. https://doi.org/10.1093/aob/mcv015.
Peltoniemi, M., Aurela, M., Böttcher, K., Kolari, P., Loehr, J., Hokkanen, T., Karhu, J., Linkosalmi, M., Tanis, C.M., Metsämäki, S., Tuovinen, J.-P., Vesala, T., Arslan, A.N., 2018. Networked web-cameras monitor congruent seasonal development of birches with phenological field observations. Agric. For. Meteorol. 249, 335–347. https://doi.org/10.1016/j.agrformet.2017.10.008.
Peng, D., Wu, C., Li, C., Zhang, X., Liu, Z., Ye, H., Luo, S., Liu, X., Hu, Y., Fang, B., 2017a. Spring green-up phenology products derived from MODIS NDVI and EVI: intercomparison, interpretation and validation using National Phenology Network and AmeriFlux observations. Ecol. Indic. 77, 323–336. https://doi.org/10.1016/j.ecolind.2017.02.024.
Peng, D., Zhang, X., Wu, C., Huang, W., Gonsamo, A., Huete, A.R., Didan, K., Tan, B., Liu, X., Zhang, B., 2017b. Intercomparison and evaluation of spring phenology products using National Phenology Network and AmeriFlux observations in the contiguous United States. Agric. For. Meteorol. 242, 33–46. https://doi.org/10.1016/j.agrformet.2017.04.009.
Peng, D., Zhang, X., Zhang, B., Liu, L., Liu, X., Huete, A.R., Huang, W., Wang, S., Luo, S., Zhang, X., Zhang, H., 2017c. Scaling effects on spring phenology detections from MODIS data at multiple spatial resolutions over the contiguous United States. ISPRS J. Photogramm. Remote Sens. 132, 185–198. https://doi.org/10.1016/j.isprsjprs.2017.09.002.
Peng, J., Wu, C., Zhang, X., Wang, X., Gonsamo, A., 2019. Satellite detection of cumulative and lagged effects of drought on autumn leaf senescence over the Northern Hemisphere. Global Change Biol. 25, 2174–2188. https://doi.org/10.1111/gcb.14627.
Piao, S., Friedlingstein, P., Ciais, P., Viovy, N., Demarty, J., 2007. Growing season extension and its impact on terrestrial carbon cycle in the Northern Hemisphere over the past 2 decades. Global Biogeochem. Cycles 21, GB3018. https://doi.org/10.1029/2006GB002888.
Piao, S., Liu, Q., Chen, A., Janssens, I.A., Fu, Y., Dai, J., Liu, L., Lian, X., Shen, M., Zhu, X., 2019. Plant phenology and global climate change: current progresses and challenges. Global Change Biol. 25, 1922–1940. https://doi.org/10.1111/gcb.14619.
Piao, S.L., Ciais, P., Friedlingstein, P., Peylin, P., Reichstein, M., Luyssaert, S., Margolis, H., Fang, J.Y., Barr, A., Chen, A.P., Grelle, A., Hollinger, D.Y., Laurila, T., Lindroth, A., Richardson, A.D., Vesala, T., 2008. Net carbon dioxide losses of northern ecosystems in response to autumn warming. Nature 451, 49–53. https://doi.org/10.1038/nature06444.
Pinty, B., Verstraete, M.M., 1992. GEMI: a non-linear index to monitor global vegetation from satellites. Vegetatio 101, 15–20. https://doi.org/10.2307/20046174.
Poorter, H., Niinemets, Ü., Poorter, L., Wright, I.J., Villar, R., 2009. Causes and consequences of variation in leaf mass per area (LMA): a meta-analysis. New Phytol. 182, 565–588. https://doi.org/10.1111/j.1469-8137.2009.02830.x.
Richardson, A.D., Keenan, T.F., Migliavacca, M., Ryu, Y., Sonnentag, O., Toomey, M., 2013a. Climate change, phenology, and phenological control of vegetation feedbacks to the climate system. Agric. For. Meteorol. 169, 156–173. https://doi.org/10.1016/j.agrformet.2012.09.012.
Richardson, A.D., Klosterman, S., Toomey, M., 2013b. Near-surface sensor-derived phenology. Editor In: Schwartz, M. (Ed.), Phenology: an Integrative Environmental Science. Springer, Dordrecht, pp. 413–430.
Rocha, A., Shaver, G., 2009. Advantages of a two band EVI calculated from solar and photosynthetically active radiation fluxes. Agric. For. Meteorol. 149, 1560–1563. https://doi.org/10.1016/j.agrformet.2009.03.016.
Rodriguez-Galiano, V.F., Dash, J., Atkinson, P.M., 2015. Intercomparison of satellite sensor land surface phenology and ground phenology in Europe. Geophys. Res. Lett. 42, 2253–2260. https://doi.org/10.1002/2015GL063586.
Ross, J., Sulev, M., 2000. Sources of errors in measurements of par. Agric. For. Meteorol. 100, 103–125. https://doi.org/10.1016/s0168-1923(99)00144-6.
Rouse Jr, J.W., Haas, R.H., Schell, J.A., Deering, D.W., 1974. Monitoring Vegetation Systems in the Great Plains With ERTS. Nasa Special Publication, pp. 309–317.
Schaaf, C. and Wang, Z., 2015. MCD43A4 MODIS/Terra+Aqua BRDF/Albedo Nadir BRDF Adjusted Reflectance Daily L3 Global 500m SIN Grid V006. NASA EOSDIS Land Processes DAAC. 10.5067/MODIS/MCD43A4.006.
Soudani, K., Hmimina, G., Delpierre, N., Pontailler, J.Y., Aubinet, M., Bonal, D., Caquet, B., de Grandcourt, A., Burban, B., Flechard, C., Guyon, D., Granier, A., Gross, P., Heinesh, B., Longdoz, B., Loustau, D., Moureaux, C., Ourcival, J.M., Rambal, S., Saint André, L., Dufrêne, E., 2012. Ground-based network of NDVI measurements for tracking temporal dynamics of canopy structure and vegetation phenology in different biomes. Remote Sens. Environ. 123, 234–245. https://doi.org/10.1016/j.rse.2012.03.012.
Studer, S., Stöckli, R., Appenzeller, C., Vidale, P.L., 2007. A comparative study of satellite and ground-based phenology. Int. J. Biometeorol. 51, 405–414. https://doi.org/10.1007/s00484-006-0080-5.
Testa, S., Soudani, K., Boschetti, L., Borgogno Mondino, E., 2018. MODIS-derived EVI, NDVI and WDRVI time series to estimate phenological metrics in French deciduous

forests. Int. J. Appl. Earth Obs. Geoinf. 64, 132–144. https://doi.org/10.1016/j.jag.2017.08.006.

Vermote, E., 2015. MOD09A1 MODIS/Terra Surface Reflectance 8-Day L3 Global 500m SIN Grid V006. NASA EOSDIS Land Processes DAAC. 10.5067/MODIS/MOD09A1.006.

Wang, C., 2006. Biomass allometric equations for 10 co-occurring tree species in Chinese temperate forests. For. Ecol. Manage. 222, 9–16. https://doi.org/10.1016/j.foreco.2005.10.074.

Wang, Q., Iio, A., Kakubari, Y., 2008. Broadband simple ratio closely traced seasonal trajectory of canopy photosynthetic capacity. Geophys. Res. Lett. 35, L07401. https://doi.org/10.1029/2008GL033619.

Wang, X.C., Liu, F., Wang, C.K., 2019. Towards a standardized protocol for measuring leaf area index in deciduous forests with litterfall collection. For. Ecol. Manage. 447, 87–94.

Wang, X.C., Wang, C.K., Guo, Q.X., Wang, J., 2016. Improving the CO_2 storage measurements with a single profile system in a tall-dense-canopy temperate forest. Agric. For. Meteorol. 228-229, 327–338. https://doi.org/10.1016/j.agrformet.2016.07.020.

White, K., Pontius, J., Schaberg, P., 2014. Remote sensing of spring phenology in northeastern forests: a comparison of methods, field metrics and sources of uncertainty. Remote Sens. Environ. 148, 97–107. https://doi.org/10.1016/j.rse.2014.03.017.

Wilson, T.B., Meyers, T.P., 2007. Determining vegetation indices from solar and photosynthetically active radiation fluxes. Agric. For. Meteorol. 144, 160–179. https://doi.org/10.1016/j.agrformet.2007.04.001.

Zhang, X., Friedl, M.A., Schaaf, C.B., 2006. Global vegetation phenology from Moderate Resolution Imaging Spectroradiometer (MODIS): evaluation of global patterns and comparison with in situ measurements. J. Geophys. Res. Biogeosci. 111, G04017. https://doi.org/10.1029/2006JG000217.

Zhang, X., Friedl, M.A., Schaaf, C.B., 2009. Sensitivity of vegetation phenology detection to the temporal resolution of satellite data. Int. J. Remote Sens. 30, 2061–2074. https://doi.org/10.1080/01431160802549237.

Zohner, C.M., Rockinger, A., Renner, S.S., 2019. Increased autumn productivity permits temperate trees to compensate for spring frost damage. New Phytol. 221, 789–795. https://doi.org/10.1111/nph.15445.